IEEE Access
Multidisciplinary | Rapid Review | Open Access Journal

Received November 10, 2018, accepted December 1, 2018, date of publication December 11, 2018,
date of current version January 7, 2019.

Digital Object Identifier 10.1109/ACCESS.2018.2886225

Mitigating the Impact of Renewable Variability With Demand-Side Resources Considering Communication and Cyber Security Limitations

DESONG BIAN[1], (Member, IEEE), DI SHI[1], (Senior Member, IEEE), MANISA PIPATTANASOMPORN[2], (Senior Member, IEEE), MURAT KUZLU[3], (Senior Member, IEEE), AND SAIFUR RAHMAN[2], (Fellow, IEEE)

[1]GEIRI North America, San Jose, CA 95134, USA
[2]Virginia Polytechnic Institute and State University, Arlington, VA 22203, USA
[3]Old Dominion University, Norfolk, VA 23529, USA

Corresponding author: Desong Bian (desong.bian@geirina.net)

This work was supported by the SGCC Science and Technology Program under the Project "Distributed High-Speed Frequency Control in UHVDC Bipolar Blocking Fault Scenario."

ABSTRACT With the rapid development of smart grid, the penetration of renewable energy resources is higher than ever and keeps growing. However, the output of renewable energy units, such as solar photovoltaics and wind turbines, is characterized by sudden and unpredictable changes. This paper proposes a novel electrical peak demand curtailment allocation (DCA) method to manage demand-side resources in response to fluctuations in renewable energy outputs. The proposed DCA method can curtail end-use loads faster than traditional demand response (DR) programs and prevent under frequency load shedding (UFLS) operation when facing sudden and unpredictable outputs of renewable energy. This DCA method considers DR potential and load curtailment priority. Case studies are conducted to demonstrate how the developed DCA method can be implemented to mitigate fluctuation in renewable outputs by curtailing electrical demand, considering communication network latency. This paper also evaluates the impact of applying different cybersecurity encryption methods on DCA operation. The simulation results prove that the developed DCA method can mitigate the impact of renewable energy fluctuation and respond fast enough to avoid traditional UFLS operation.

INDEX TERMS Renewable mitigation, demand curtailment allocation, communication networks, cybersecurity, latency.

I. INTRODUCTION

This High penetration of renewable energy resources makes grid operation a challenging task. It is difficult to keep the balance between supply and demand for electricity with highly fluctuated renewable energy output. Thus, mitigating renewable impacts draws lots of attention. In addition to the use of battery energy storage to mitigate renewable energy variability, several methods are being deployed to manage demand-side resources, such as various types of DR programs, or to shed the load under emergencies, such as UFLS. Managing demand-side resources with the presence of renewables is the topic of interest of this paper.

Without high renewable penetration, the current practice to alleviate power system stress conditions in hot summer days is to implement DR, as peak load days can be predicted in advance. As a result, electric utilities in the U.S. have introduced diverse types of DR programs – both time-based DR and incentive-based DR programs [1], [2]. Time-based DR programs are achieved in response to electricity prices, which are usually announced one day ahead. For example, DR programs offered by California Independent System Operator (CAISO) [3] are triggered based on various conditions, such as day-ahead forecasted temperature, day-ahead forecasted demand and high price forecasts. One popular incentive-based DR program, known as an emergency demand response program (EDRP), can alleviate power system stress conditions by reducing load at customer premises. EDRP usually needs an advance notice of at least two hours. As introduced in [4] and [5], New York Independent System Operator (NYISO)'s EDRP requires day-ahead or two-hour ahead for advance notification.

However, with the increasing penetration of renewable energy sources, the sudden loss of renewable energy output may lead to insufficient generation to keep up with the demand for electricity in certain periods. Since DR program requires at least two hours for customer notification, traditional DR implementation is not a suitable means to mitigate fluctuation in renewable energy sources. Typically, in an event where there is a sharp decrease of renewable energy, causing a significant drop in power system frequency, UFLS is activated to curtail part of system load fast enough to mitigate renewable impacts on power system (e.g., to recover the system frequency back to its nominal value). Usually, its response time is within a fraction of a second. Despite the fact that UFLS can curtail a large number of loads within a very short period of time, it comes at the cost of large load lost [6], [7]. As a result, UFLS should be deployed as the last resource when facing a sudden and significant drop in renewables.

To fill the gap of traditional DR and UFLS programs, researchers [8]–[11] have proposed methods to mitigate renewable penetration and keep the system operating within its normal frequency range. In [8], a strategy for supporting high penetration of renewable generation via implementation of real-time electricity pricing and demand response is introduced. A frequency regulation control strategy for wind-power generation system with flywheel energy storage unit is presented in [9]. Ma and Chowdhury [10] also consider wind power generators for the frequency regulation by applying combined control strategy. A novel DCA method – which is an expert-based demand curtailment allocation approach using Analytic Hierarchy Process (AHP) method that has the ability to respond faster than DR programs and avoid UFLS operation – is introduced in [11]. This paper extends the application of DCA method previously proposed by authors to mitigate fluctuation of large-scale renewable output with the presence of communication and cyber security limitations.

All above DR programs and other renewable mitigation solutions rely on two-way communication networks to deliver end-user usage information and DR signals from the system operator. Besides, to protect end-user customers' privacy and to provide a fast and stable communication, a secure and reliable communication network is necessary. Applying cybersecurity technologies, such as encryption methods, to prevent adversary attacks can protect customers' privacy and allow the smart grid to operate reliably. Nonetheless, implementing encryption methods requires extra software and hardware, which increases the complexity of the system and extends the system latency. Therefore, it is necessary to analyze the limitation of using encryption methods on the smart grid operation.

Hence, the contribution of this paper – in addition to extending the application of DCA method to mitigate renewable fluctuation – also includes evaluating the capability of a communication network to support smart grid applications and analyzing limitations of implementing different encryption methods on the DCA strategy operation. This is to prove that the operation of the DCA can function quickly enough to avoid the operation of UFLS considering the background communication traffic from popular smart grid applications that share the same network.

II. THE DCA ALGORITHM

In this section, the DCA algorithm is discussed. The DCA algorithm was originally developed by the current authors [11] to allocate demand curtailments (MW) among distribution substations (DS) in an electric utility service area. Its application is extended in this paper to mitigate the impact of high renewable energy penetration levels.

DCA is quantified considering DR potential and load curtailment priority of each DS, which can be determined using DS loading level, the capacity of each DS, customer types and load categories (deployable, interruptible or critical). AHP is used to model a complex decision-making process according to expert inputs and objective parameters. The DCA algorithm is briefly described below. Interested readers are encouraged to refer to [11] for the detailed discussion of the DCA algorithm.

A. DCA ALGORITHM

The DCA algorithm starts by retrieving the information at each DS every fixed time interval, e.g., 15 minutes. The information to be retrieved includes DS capacity, load (MW) by category (i.e., residential/commercial), load (MW) by classification (i.e., deferrable/interruptible/ critical) and forecasted loading level of each DS. It is assumed that a demand curtailment request (MW) is sent from an ISO/RTO. Once a curtailment request is received, the first-step curtailment process is initiated.

The first-step curtailment process starts by comparing the requested demand curtailment amount (MW) with the total amount of all deferrable and interruptible loads in the curtailment-requested service area, which can span multiple DSs. If the requested amount is equal or larger than the sum of deferrable and interruptible loads, all deferrable and interruptible loads will be curtailed first, and the balance will come from demand response at the customer level.

The second-step curtailment process will be initiated: (1) to manage the remaining curtailment requested amount; or (2) to manage the original curtailment requested an amount that is less than deferrable loads. This step is to allocate the (remaining) requested demand curtailment amount among different DSs based on their curtailment priority factor, which is determined using 3-level AHP depicted in Figure. 1. Outcomes of AHP are curtailment allocation to each DS. If the curtailment amount allocated to a particular DS is larger than its sum of deferrable and interruptible loads, the curtailment contribution of that particular DS will be set equal to its sum of deferrable and interruptible loads; and the remaining amount will be reallocated to other DSs.

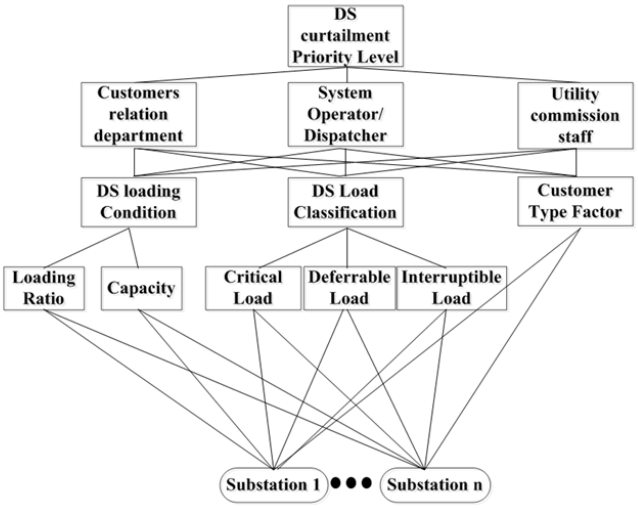

FIGURE 1. Three-level AHP structure.

B. DETERMINATION OF CURTAILMENT PRIORITY FACTOR

A 3-level AHP method is used to determine the curtailment percentage of each DS. Decision criteria have three levels as explained below and the detailed relationship is shown in Figure. 1.

The 1st-level criteria involve three distinct groups of experts' judgments, representing the weight of their opinions. In this study, experts are from customer relation department, system operators/dispatchers, and utility commission staff. Note that in using the AHP method, relative importance – as given by various experts – is used as opposed to their absolute judgments. Thus, the unlikely off-scale remark by one expert will not skew results. The 2nd-level criteria are criteria related to each DS, including DS loading condition, load classification and customer type factor.

The 3rd-level criteria expand the above criteria as follows: (i) DS loading condition including DS loading ratio and its capacity; (ii) DS load classification including critical/ deferrable and interruptible loads; and (iii) Customer type factor (CTF) are used to present the importance of DS's customers in different time periods. Deferrable loads are those that can be deferred from peak hours and can be deployed any time during off-peak hours. Interruptible loads are those that can be interrupted momentarily. Load compensation may be necessary as soon as a DR event ends. Critical loads are those that are non-deferrable and non-interruptible. This paper considers both residential and commercial customers for demand curtailment allocation.

III. THE STRATEGY OF OPERATION, COMMUNICATION NETWORKS AND ENCRYPTION FOR DCA IMPLEMENTATION

This section discusses the strategy of DCA operation, communication networks and encryption methods which were implemented to evaluate the developed DCA algorithm.

A. THE STRATEGY OF DCA OPERATION

The smart grid involves many different applications. In the proposed framework, the smart grid operation status is classified into Normal, Demand Response (DR) event, Demand Curtailment Allocation Strategy (DC) event and Emergency (E) event. The DCA algorithm is activated when a traditional DR program cannot fulfill the demand curtailment request either the operation time left is insufficient (e.g., shorter than two hours) or a DR event cannot provide enough curtailment to keep the system within its normal operation. UFLS only operates when DCA cannot fully handle the curtailment request. The transition among these statues is shown in Figure. 2.

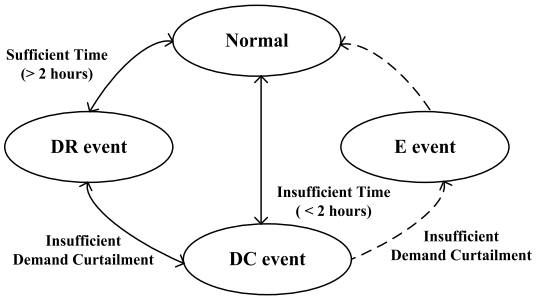

FIGURE 2. Power grid operation status.

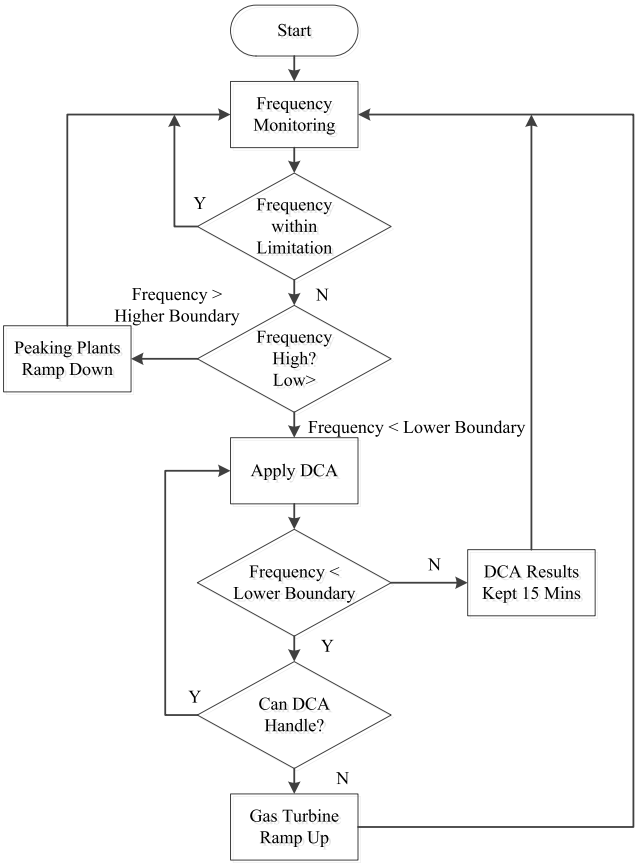

FIGURE 3. The operation of the DCA.

The DCA operation process is depicted in Figure. 3. During a power system normal operating condition, the system load is served by both traditional and renewable energy (e.g., PV) power plants. A central control center continuously

monitors the system frequency. Once the frequency is out of its normal operation range, specific actions are taken. As shown in Figure. 3, load curtailment is initiated using the DCA method if the system frequency decreases below a certain threshold. In case the DCA operation cannot help maintaining nominal system operating frequency, peaking power plants are used to supplement DCA operation.

B. COMMUNICATION NETWORKS FOR DCA

DR implementation requires two-way communications between the control center and end-user customers. That is, it needs data from end-use customers to make a decision; and once the decision is made, the decision needs to be communicated back to end-use customers. Achieving two-way communications requires the following steps: (1) the information from end-use customers collected by smart meters is sent to a local data concentrator; (2) a local data concentrator forwards the information to a base station; (3) the base station packages the information and sends to the control center; and (4) the decision from the control center is sent to end-use customers in a reverse direction.

To realize this two-way communication, three layers of smart grid communication networks (i.e., WAN-wide area network, NAN-neighborhood area network and premise area network) are necessary. While WAN facilitates information exchange between the control center and base stations, NAN allows information exchange between base stations and end-user customers through local data concentrators. The premise area network facilitates the control of smart appliances inside smart home/buildings.

Among different smart grid infrastructures, the advanced metering infrastructure (AMI) has potential to enable demand response implementation as it covers both WAN and NAN and includes necessary building blocks, such as base stations, local data concentrators, etc. Therefore, the communication network supporting AMI applications is used as a basis to simulate DR implementation in this paper. On the other hand, within a home, a HEM (home energy management) system is widely used to enable automated DR applications at the customer premise. A HEM can provide the homeowner/building operator the ability to automatically perform smart load controls based on utility signals, as well as customer preference and load priority.

The whole network structure for DCA implementation is shown in Figure. 4.

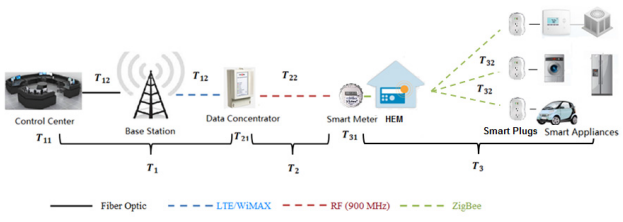

FIGURE 4. The network structure for DCA implementation.

As shown in (1), the latency (T_i) for transmitting a command within any network comprises: the communication delay (T_{icomm}) and the DCA algorithm processing delay (T_{iDCA}). According to Figure. 4, T1, T2 and T3 represent the latency in the WAN, NAN and HAN networks, respectively.

$$T_i = T_{iDCA} + T_{icomm} \tag{1}$$

The communication delay (T_{icomm}) can be further divided into: transmission delay (T_{itran}), propagation delay (T_{iprop}) and processing delay (T_{iproc}). See (2).

$$T_{icomm} = T_{itran} + T_{iprop} + T_{iproc} \tag{2}$$

Hence, the overall network latency (T_{total}) is calculated by adding the latency of all three network layers, i.e., WAN, NAN and LAN, as shown in (3).

$$T_{total} = \sum_{i=1}^{3} T_i \tag{3}$$

C. ENCRYPTION METHODS FOR THE PROPOSED DCA STRATEGY

Data Encryption Standard (DES), Triple DES (3DES), Advanced Encryption Standard (AES), Rivest-Shamir-Adleman (RSA) and Blowfish are five popular encryption methods. Since the DES method is not secure [12] and the RSA method has slow performance [13], this paper focuses on analyzing how: 3DES, AES and Blowfish impact DCA operation in terms of additional processing and transmission delays caused by implementing these encryption methods on the DCA strategy.

All three encryption methods are block-cipher which operates on a fixed length (block size) string of bits. Key size is the number of bits in a key used by the encryption method. The parameters for each type of these encryption methods are listed in Table 1.

TABLE 1. Parameters of encryption methods.

	3DES	AES	Blowfish
Block Size (bit)	64	128	64
Key Size (bit)	128	128	64

IV. CASE STUDY ASSUMPTIONS AND DESCRIPTION

Case studies are demonstrated to compare the performance of the developed DCA strategy in mitigating renewable energy fluctuation, that operates on an AMI network using three different encryption methods. The IEEE 14-bus system model is simulated in the PowerWorld simulator.

A. POWER SYSTEM ASSUMPTIONS

Assumption 1 (Power Network): The IEEE 14-bus system model used for this simulation study is shown in Figure. 5. This system consists of five synchronous machines, three of which are synchronous compensators used only for reactive power support. There are 11 load points in the system totaling 259 MW and 81.3 MVAR. Its normal operating frequency is at 60 Hz.

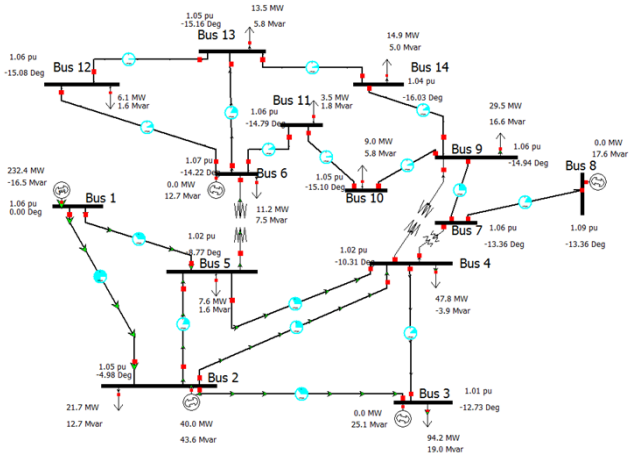

FIGURE 5. The IEEE 14-bus system model.

Assumption 2 (Fossil Fuel Ramp Rate): The average ramp rate of a generator is defined as the change in load served divided by the amount of time required to move from the initial load to the final load. Ramp rates of most industrial frame gas turbine models are advertised as 10 MW/minute up to 100 MW/minute, with an average of about 25 MW/minute [14]. For example, GE 7F.05 gas turbine's ramp rate is 40 MW/minute. GE 7FA gas turbine's ramp rate is 30 MW/minute [15]. Siemens SGT6-5000F gas turbine's ramp rate is up to 40 MW/minute [16] and Siemens H class CCGT (combined-cycle gas turbine) ramp rate is 25 MW/minute [17]. Ramp rates of traditional generation (coal/steam) of different unit sizes (76, 155, 350MW) vary from 2 to 4 MW/minute [18]. Based on the size of generation in IEEE 14-bus system, the ramp down rate of coal/steam units is assumed at 3.5 MW/minute. The gas turbine is used as backup generation and its ramp rate is assumed at 25 MW/minute.

Assumption 3 (Power System Frequency Response): a) Western Electricity Coordinating Council (WECC) Category B/C Standard

WECC is geographically the largest and most diverse of the eight regional entities with delegated authority from the North American Electric Reliability Corporation (NERC) and Federal Energy Regulatory Commission (FERC). It provides an environment for the development of reliability standards. WECC Category B Frequency monitors all load buses for a frequency dip below 59.6 Hz for a duration of 0.1 seconds (6 cycles) [19]. Similarly, WECC Category C Frequency monitors all load buses for a frequency dip below 59.0 Hz for a duration of 0.1 seconds (6 cycles) [20].

In this study, the proposed DCA method is triggered when the grid frequency falls into the WECC Category B Frequency monitoring condition. If the DCA is not able to draw the frequency back to its normal range and the frequency drops into the WECC Category C Frequency monitoring condition, the UFLC program is triggered.

b) Frequency Response

Power system frequency is a continuously changing variable, and it is determined and controlled by the balance between system demand and total supply. The frequency falls when the demand is greater than the supply. To keep the system's frequency within its normal operating limits, it is necessary to be aware of the system's frequency response (MW/0.1 Hz). Frequency response is a measure of a system's ability to stabilize frequency immediately following the sudden loss of generation or load. It is defined as the sum of the change in demand and the change in generation, divided by the change in frequency, expressed in MW/0.1 Hz [21]. In practice, the amount of frequency decline depends on characteristics of the load and generators available at the time [22]. Quantifying the frequency response of a system is typically accomplished by observing frequency decline events. For example, the NERC Resources Subcommittee occasionally requests Frequency Response Characteristic Surveys for specific events [19].

To estimate the frequency response ratio of the IEEE 14-bus system model used in this section, several frequency decline cases are simulated. For example, the frequency of the system decreases from 60 Hz to 58.5 Hz when the load increased 40 MW. Using (4), the IEEE 14-bus system's frequency response is determined at 27.1 MW/0.1 Hz.

$$k_p = -\left(\frac{f_1 - f_0}{L_1 - L_0}\right) \tag{4}$$

B. LOAD AND RENEWABLE ENERGY ASSUMPTIONS

Assumption 1 (Load profile): The load data used in case studies are derived from distribution feeders in a service area of an electric utility in Virginia. The data is available at one-minute intervals, and the day selected for the case study is a typical summer day in August. The system load is scaled up so that its peak is 259 MW, which is the steady state load value of the IEEE 14-bus system. The derived load data for a typical summer day on IEEE 14-bus system is also shown in Figure. 6.

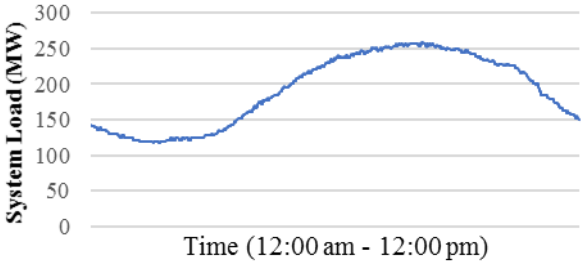

FIGURE 6. The load (MW) of a typical summer day.

Assumption 2 (PV output): The solar PV output used in this study is derived based on the data from the 6.4kW solar PV station located on the rooftop of Virginia Tech Research

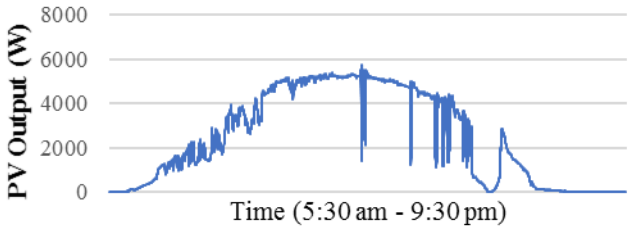

FIGURE 7. The solar power (W) output.

TABLE 2. Characteristics of selected smart grid applications.

	Package Size (bytes)	Data Sampling Frequency (Times per day)	Latency (second)	Reliability (%)
DCA	100	As needed	< 5	>99.5
DR	100	1 per event	< 60	>99.5
Pricing	100	2-6	< 60	>98
Metering (1)	100	As needed	< 15	>98
Metering (2)	1600 - 2400	4-6 per residential; 12-24 commercial	< 4 hours	>98
EV	100	2-4	< 15	>98

Center in Arlington, VA, which is available 15-second intervals. An example of the 15-second PV power output between 5:30 am and 9:30 pm is shown in Figure.7.

In the case study, the PV unit is assumed to be located at Bus 2 of the power system in Figure. 5. The size of PV unit is scaled up in the case study to study the impact of different PV penetration levels on DCA operation. The PV sizing assumption is discussed below.

Assumption 3 (PV penetration Level): In this study, the PV penetration level (PV_{pene}) is defined as the ratio of total peak power generated by PV panels (P_{pv}) to the peak load apparent power on the feeder (P_{load}). See (5).

$$PV_{pene} = \frac{P_{pv}}{P_{load}} \tag{5}$$

This study looks at various PV penetration levels, i.e., 10% and 20% and analyzes how the DCA method is capable of mitigating the impact of different PV penetration levels.

C. SMART GRID APPLICATIONS

Since many smart grid applications share the same communication network, and each smart grid application has distinctive characteristics, e.g., data size, data sampling frequency, latency and reliability requirements, it is necessary to ensure proper operation of all smart grid applications especially those sharing the same network. Characteristics of the proposed DCA method, as well as those of other popular smart grid applications, are summarized in Table 2.

DR allows a utility to talk to devices at customer premises. Pricing applications involve broadcasting of price information to meters and devices. Meter reading allows a utility to collect data from electric/gas/water meters and transfer data to a central database for billing and analysis. Two kinds of metering applications are considered: (1) on-demand meter reading and (2) meter reading with scheduled time intervals (15-minute or hours). Electric transportation applications involve both electricity flow from vehicles to the power grid (vehicle-to-grid, V2G) and electricity flow from the power grid to vehicles (grid-to-vehicle, G2V).

V. ANALYZING DELAYS FROM COMMUNICATION NETWORKS, DCA ALGORITHM AND ENCRYPTION SECURITY

This section describes communication network simulation using OPNET network simulator to derive communication delays in WAN, NAN and HAN when implementing DCA strategy. It also summarizes DCA algorithm delay and discusses encryption security delay.

A. COMMUNICATION DELAY

1) COMMUNICATION DELAY IN WAN AND NAN

Since the DCA strategy is mainly implemented in NAN and WAN, this section discusses network components and structures that support its implementation and their corresponding communication delay.

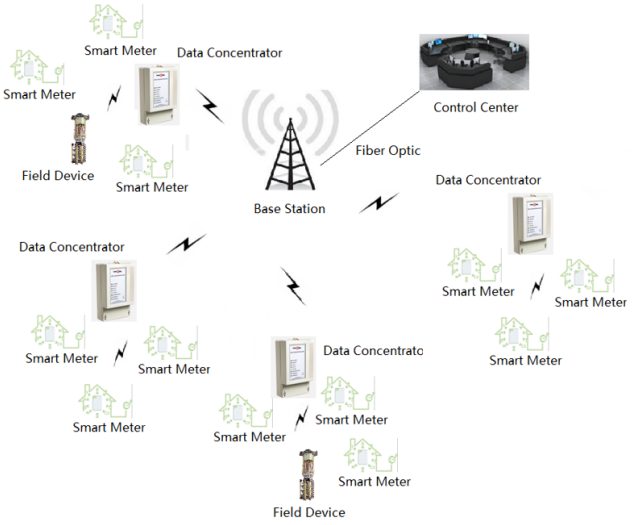

FIGURE 8. Communication networks supporting smart grid applications.

The network as shown in Figure. 8 illustrates the communication network structure that supports the AMI application. Supporting a large number of smart meters and field devices, network components including several data concentrators, base stations and a control center. AMI network has two major parts. One is the AMI backbone network, i.e., communications between the control center and base stations. The other is the AMI smart meter network, i.e., communications among base stations, data concentrators and smart meters.

Based on the survey of communication schemes deployed in real-world AMI projects presented in [23], the fiber optic and WiMAX/LTE are the most popular communication technologies supporting the AMI backbone network. Between two choices, the fiber optic option has an advantage over the

WiMAX/LTE option in that it can provide higher bandwidth. Furthermore, the fiber optic technology can provide higher reliability level than WiMAX /LTE during inclement weather conditions.

For the AMI smart meter network, the 900 MHz mesh network appears to be the most popular technology choice. This is because it has good reliability and flexibility performance. In addition, the implementation cost of 900 MHz mesh network is relatively inexpensive as it can rely on an existing infrastructure. According to [24], the 900 MHz RF network's data rate can be up to 13.5 Mbps. Besides, its coverage is around 25 miles. For each base station, it allows 300-1000 customers to access.

For the simulation, an AMI network is set up in OPNET, comprising 15 base stations, 690 data concentrators and 264,000 smart meters as shown in Figure. 9.

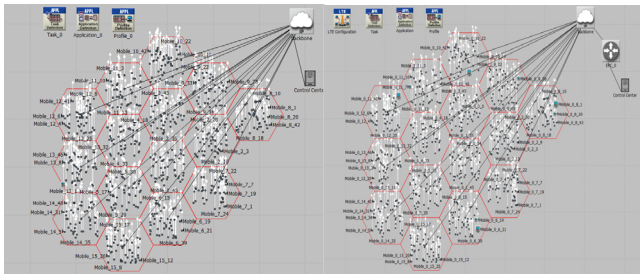

(a) (b)

FIGURE 9. Simulate AMI networks in OPNET. (a) Fiber optic – WiMAX. (b) Fiber optic – LTE.

To calculate the latency in the AMI network, it is assumed that a smart meter and a data concentrator have the same access speed, shown in (6).

$$T_{tran} = T_{proc} = \frac{S_p \bullet N_c}{R} \tag{6}$$

where:

S_p - the size of the package (bits);
N_c - the number of customers;
R - the data rate (bps).

To calculate the propagation delay (7), the distance between each access points and the base station is assumed to be Gaussian distribution. And the propagation speed of the signal in free space is the same as that of light speed which is 3∗10^8 m/s.

$$T_{prop} = \frac{D}{S_{prop}} \tag{7}$$

where:

D - the distance (m);
S_{prop} - the propagation speed (m/s).

The worst-case scenario is when the developed DCA functions during the operation of all other smart grid applications. The worst-case scenario was simulated in OPNET to determine latency from communication networks, and the results are summarized in Table 3.

TABLE 3. Latency from communication networks (WAN and NAN).

	Backbone Network (s)		Smart Meter Network (s)
	Fiber-optic WiMAX	Fiber-optic LTE	900 MHz RF
Latency (second)	< 0.06	< 0.05	< 0.02

TABLE 4. Latency from HAN.

Communication Technologies	ZigBee	Wi-Fi	Ethernet
Latency (second)	0.0249 - 0.1146	0.0107 - 0.0250	0.0005 - 0.0009

TABLE 5. The overall communication delay.

	T_{icomm} (WAN)	T_{2comm} (NAN)	T_{3comm} (HAN)
Latency (second)	< 0.1	< 0.1	< 0.1

TABLE 6. Processing speed of encryption methods.

	3DES	AES	Blowfish
Encryption (Mbytes/Second)	3.450	4.174	25.892
Decryption (Mbytes/Second)	5.665	6.452	18.72

2) COMMUNICATION DELAY DUE TO HAN

Load control implementation within a smart home relies on the HEM system. Communication technologies of interest include ZigBee, Wi-Fi and Ethernet. These technologies were simulated in OPNET, assuming that a house has at most 15 devices to monitor and control. Their performance is compared in terms of latency, as shown in Table 4. The largest latency is around 0.11s [25].

3) OVERALL COMMUNICATION DELAY

By summing the communication latency in WAN (T1) and NAN (T2) based on Table 3, and the latency in HAN (T3) based on Table 4, the overall communication delay can be obtained. Table 5 shows that the communication latency in each network is less than 0.1 second. Since multiple testing cases are implemented, only the upbound are provided. Hence, the overall communication delay of all three networks is less than 0.3 seconds.

B. DCA ALGORITHM DELAY

The DCA algorithm was set up on one PC with CPU of 2.4 GHz and 2 GB RAM. The latency of the DCA algorithm progress was measured and it was less than 0.1 second.

C. ENCRYPTION SECURITY DELAY

The processing speed of the encryption method is another important factor. According to [26], the encryption and decryption processing speed on a PC with CPU (2.4 GHz and 2 GB RAM) are listed in Table 6.

It is assumed that each information packet has 100 bytes. For DCA operation, the total data throughput is around 50 Mbits. As a result, at the control center, the encryption throughput is considered as 50 Mbits. At the data concentrator, the decryption throughput for the received information

TABLE 7. Processing latency for three encryption methods.

	3DES		AES		Blowfish	
	Encryption	Decryption	Encryption	Decryption	Encryption	Decryption
WAN-NAN	1.811	0.024	1.497	0.021	0.241	0.007
NAN-HAN	0.012	1.765 E-05	0.010	1.549 E-05	0.002	5.341 E-06
Sum	1.8479		1.5286		0.250	

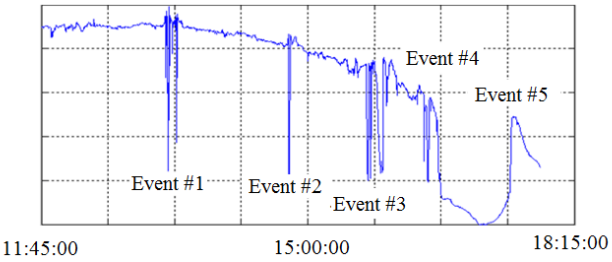

FIGURE 10. Solar PV output in the afternoon of a typical summer day.

from the control center is around 1.08 Mbits. To forward the information, another encryption processing is needed. And the encryption throughput is 423∗100 bytes. And the decryption throughput at home site is around 100 bytes. The encryption methods' processing latency is calculated using (8) and summarized in Table 7.

$$T_{cyber} = \frac{P}{R} \tag{8}$$

where:

T_{cyber} - the latency of encryption or decryption processing (s);
P - the data throughput (bits);
R - the processing speed of encryption or decryption (bits/second).

VI. PERFORMANCE OF DCA ALGORITHM TO MITIGATE RENEWABLE ENERGY FLUCTUATION

Given delays from the communication network, DCA algorithm processing and encryption security discussed in Section V, this section analyzes the performance of DCA in mitigating renewable energy fluctuation when three different encryption methods (3DES, AES and Blowfish) are implemented. Figure. 10 depicts the solar PV output during the afternoon of a typical summer day.

As shown there are five significant and sudden changes in solar PV output. Table 8 summarizes these solar power output changes at two different solar PV penetration levels, i.e., 10% and 20%, together with the system load (MW) at the time of sudden PV output changes.

While Events #1, #2, #3 and #4 represent sudden decreases in solar PV outputs, Event #5 represents a sudden increase in solar PV output. It can be seen that the drop in PV output in Event #1 is considered the largest among all five events in Table 8. That is, the PV output drop at 20% PV penetration is as high as 15.3% of the coincident system

TABLE 8. Description of solar PV outputs.

Event#	Time	System Load (MW)	The Max of PV output drop (MW)	
			10% Penetration	20% Penetration
1	13:17:30	238	18.2	36.4
2	14:49:00	248	16.4	32.8
3	15:48:00	249	12.2	24.4
4	16:31:00	246	6.3	12.6
5	17:36:00	246.7	-8.6	-17.2

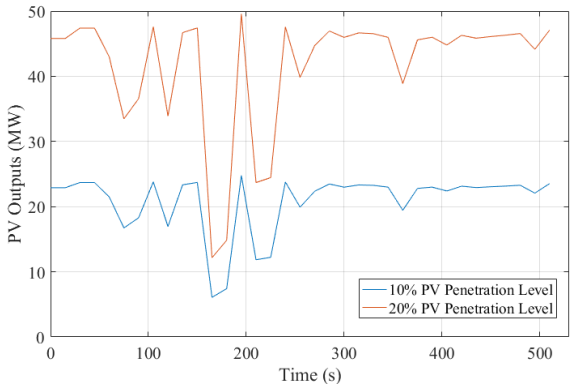

FIGURE 11. PV output during Event #1 (10% and 20% penetration levels).

load (36.4MW/238MW). Hence, this study focuses on Event#1 to explain how the DCA operation can mitigate sudden PV output changes. Note that in Event #5 the sudden increase in PV output is handled by gas turbines, not DCA.

A. EVENT #1 @ 13:17:30

Event #1 happened at 13:17:30. Figure. 11 shows the detailed PV output fluctuation during Event #1 at 10% and 20% penetration levels. The largest drop in PV output happened at around t = 166 seconds, showing the PV output dropped by 18.2 MW to around 6 MW (10% penetration) and dropped by 36.4 MW to around 12 MW (20% penetration).

Figure. 12 illustrates how the system frequency changes when the DCA with the 3DES encryption method is applied to handle sudden changes in PV output.

In the case of 10% solar penetration level with 3DES encryption method (Figure. 12(a)), changes in the system frequency can be explained as follows:

- At 13:18:30 (t = 60): as the solar output began to drop, the system frequency decreased from around 60Hz at t = 60 to 59.6Hz at t = 135. During this period, the system frequency remained within its normal operating limits, i.e., >59.6Hz.
- At 13:19:45.46 (t = 135.46): the system frequency decreased below 59.6 Hz. As a result, the DCA took action and curtailed 10.64 MW of load. At this point, the system frequency raised and remained higher than 59.6 Hz.
- At 13:19:26.76 (t = 166.76): since the solar output was as low as 6 MW, the system frequency sharply dropped below 59.6 Hz for the second time. The DCA took

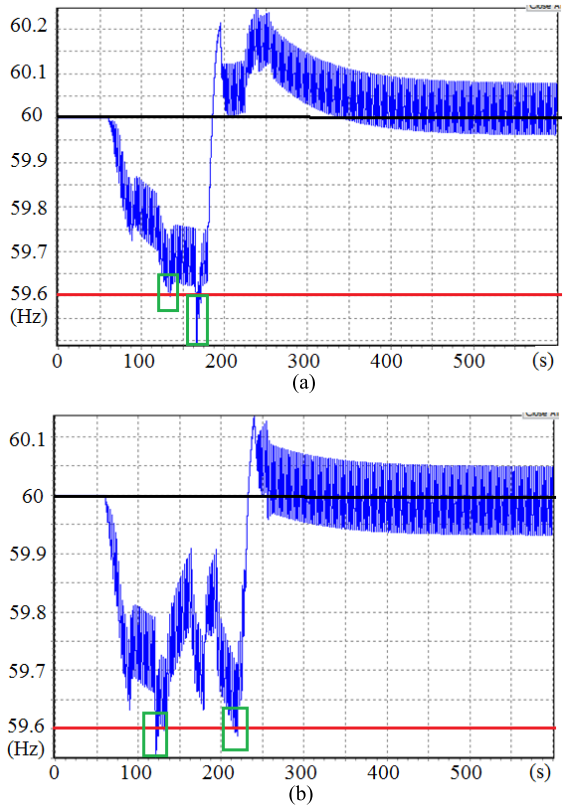

FIGURE 12. Simulation results for Event #1. (a) 3DES & 10% PV. (b) 3DES & 20% PV.

another curtailment of 10.51 MW load. Then the system frequency began to increase.

- At 13:20:49 (t = 199): the system frequency increased to around 60.2 Hz due to the increase in solar output.
- Between 13:20:50 (t = 200) and 13:21:50 (t = 260): the system frequency had some disturbances since the PV outputs had several fluctuations.
- After 13:24:00 (t >= 400): the system frequency became stable.

For the case of 20% solar penetration level with 3DES encryption method (Figure. 12(b)), changes in the system frequency can be explained as follows:

- At 13:18:30 (t = 60): as the solar output began to drop, the system frequency began to decrease from its nominal value of 60Hz, but still remained within its normal operating limits (i.e., > 59.6Hz).
- At 13:19:29.73 (t = 119.73): the system frequency began to decrease below 59.6 Hz. As a result, the DCA took action and curtailed 10.36 MW of load. After this, the system frequency became higher than 59.6 Hz.
- Between 13:19:30 (t = 120) and 13:20:50 (t = 200): there were three disturbances. It was because the solar outputs had several fluctuations. Since the system frequency was above 59.6 Hz, DCA did not take any actions.
- At 13:21:10.46 (t = 220.46): since the solar output was as low as 25 MW, the system frequency dropped below 59.6 Hz again. The DCA took another curtailment of 10.09 MW load. The system frequency began to increase.
- After 13:22:30 (t >= 300): the system frequency was steady and kept within its normal operating frequency.

Table 9 summarizes the total amount of load curtailment for Event #1 when three different encryption methods are used under two different solar penetration levels. Under the same solar penetration level, the shorter processing time required by the encryption method implies the lesser amount of load curtailment is needed. Hence, Table 9 indicates that the performance of the Blowfish method is slightly better than that of the 3DES and AES methods. Since system frequency dropped and reached the lower limit (59.6 Hz) faster in the 20% penetration level case, the total load curtailments were less than that of the 10% case for all encryption methods used.

TABLE 9. Load curtailment for event#1.

	10% Penetration	20% Penetration
3DES	21.150	20.452
AES	20.912	20.431
Blowfish	20.815	20.407

TABLE 10. Simulation results with 10% PV penetration level.

	Event #1	Event #2	Event #3	Event #4	Event #5
3DES	21.150	20.750	20.492	10.259	-6.1
AES	20.912	20.558	20.475	10.256	-6.1
Blowfish	20.815	20.525	20.465	10.250	-6.1

TABLE 11. Simulation results with 20% PV penetration level.

	Event #1	Event #2	Event #3	Event #4	Event #5
3DES	20.452	20.503	20.513	20.558	-11.5
AES	20.431	20.433	20.506	20.555	-11.5
Blowfish	20.407	20.430	20.503	20.548	-11.5

B. SUMMARY

This section summarizes case studies for all five events with different encryption methods and two PV penetration levels. The total amount of load curtailment or the amount of gas turbine ramping down (for Event #5) for each case study is summarized in Tables 10 and 11 for the 10% and 20% PV penetration levels, respectively.

It can be seen from Table 10 and 11 that 10% and 20% PV penetration level cases have similar load curtailment in all events. This is because the system frequency in the case of 20% PV penetration dropped below 59.6 Hz faster than that in the 10% PV penetration. Hence, the DCA took actions faster.

In all case studies, with DCA implementation and any of the encryption method used, the system frequency can be kept within its normal operating range with the presence of significant fluctuation in solar energy output. This proofs the effectiveness of the developed DCA method.

VII. CONCLUSION

In order to provide a remedy to the problem of sudden drop in renewable energy outputs, this paper proposes an

expert-based demand curtailment allocation approach, which is pre-calculated but dynamically readjusted, if needed. It can curtail end-use loads faster than traditional DR programs and prevent UFLS operations. The performance of the communication network supporting the DCA implementation is evaluated to determine how rapidly the proposed strategy can be implemented. Since a number of smart grid applications share the same communication network, the performance of this communication network is also evaluated considering the simultaneous operation of popular smart grid applications. Lastly, this paper also analyzes additional processing and transmission delays caused by implementing selected encryption methods (3DES, AES and Blowfish encryption methods) on the proposed demand curtailment allocation strategy.

REFERENCES

[1] (Jun. 2009). *A National Assessment of Demand Response Potential: Demand Response Potential, Staff Report, Federal Energy Regulatory Commission*. Accessed: Dec. 2018. [Online]. Available: http://www.opower.com/bdrpotential/media/FERC_demand_response_paper.pdf
[2] The Federal Energy Regulatory Commission Staff. (Jun. 17, 2010). *National Action Plan on Demand Response*. Accessed: Dec. 2018. [Online]. Available: http://www.ferc.gov/legal/staff-reports/06-17-10-demand-response.pdf
[3] CAISO. (Nov. 2007). *CAISO Demand Response Resource User Guide*. Accessed: Dec. 2018. [Online]. Available: http://www.caiso.com/Documents/DemandResponseResourceRelease1UserGuideVersion3_0.pdf
[4] Midwest ISO. (Mar. 2007). *Emergency Demand Response in PJM and the NYISO*. Accessed: Dec. 2018. [Online]. Available: https://www.naesb.org//pdf2/dsmee061807w2.pdf
[5] NYISO. *Demand Response*. Accessed: Dec. 2018. [Online]. Available: http://www.nyiso.com/public/webdocs/markets_operations/services/market_training/workshops_courses/Training_Course_Materials/NYMOC_MT_ALL_201/Demand_Response.pdf
[6] A. Apostolov. *IEEE Guide for Under Frequency Load-Shedding and Restoration*. Accessed: Dec. 2018. [Online]. Available: https://www.pacw.org/noache/issue/autumn_2008_issue/industry_reports/ieee_power_systems_relaying_committee.html
[7] NERC. *Under Frequency Load Shedding Metric*. Accessed: Dec. 2018. [Online]. Available: http://www.nerc.com/pa/RAPA/ri/Pages/UnderFrequencyLoadShedding.aspx
[8] R. Wang, Y. Xie, H. Zhang, C. Li, W. Li, and V. Terzija, "Dynamic power flow algorithm considering frequency regulation of wind power generators," *IET Renew. Power Gener.*, vol. 11, no. 8, pp. 1218–1225, Jun. 2017.
[9] J. Yao, M. Yu, W. Gao, and X. Zeng, "Frequency regulation control strategy for PMSG wind-power generation system with flywheel energy storage unit," *IET Renew. Power Gener.*, vol. 11, no. 8, pp. 1082–1093, Jun. 2017.
[10] H. T. Ma and B. H. Chowdhury, "Working towards frequency regulation with wind plants: Combined control approaches," *IET Renew. Power Gener.*, vol. 4, no. 4, pp. 308–316, Jul. 2010.
[11] D. Bian, M. Pipattanasomporn, and S. Rahman, "A human expert-based approach to electrical peak demand management," *IEEE Trans. Power Del.*, vol. 30, no. 3, pp. 1119–1127, Jun. 2015.
[12] *Encryption Algorithms*. Accessed: Dec. 2018. [Online]. Available: http://www.encryptionanddecryption.com/algorithms/encryption_algorithms.html
[13] *IEEE Standard for Local and Metropolitan Area Networks–Media Access Control (MAC) Security Amendment 1: Galois Counter Mode-Advanced Encryption Standard—256 (GCM-AES-256) Cipher Suite*, IEEE Standard 802.1AEbn-2011 (Amendment to IEEE Standard 802.1AE-2006), Oct. 2011, pp. 1–52.
[14] *Combustion Engine vs Gas Turbine: Ramp Rate*. Accessed: Dec. 2018. [Online]. Available: http://www.wartsila.com/energy/learning-center/technical-comparisons/combustion-engine-vs-gas-turbine-ramp-rate
[15] *7F.05Gas Turbine (60Hz)*. Accessed: Dec. 2018. [Online]. Available: https://powergen.gepower.com/products/heavy-duty-gas-turbines/7f-05-gas-turbine.html
[16] *Gas-Turbine-Siemens*. Accessed: Dec. 2018. [Online]. Available: http://www.energy.siemens.com/hq/pool/hq/power-generation/gas-turbines/downloads/gas-turbines-siemens.pdf
[17] *Power Engineering International*. Accessed: Dec. 2018. [Online]. Available: http://www.powerengineeringint.com/articles/print/volume-19/issue-6/features/fast-starts-and-flexibility-let-the-gas-turbine-battle-commence.html
[18] *Active Power Ramp Rate*. Accessed: Dec. 2018. [Online]. Available: http://www.neos-guide.org/sites/default/files/ramp_rates.pdf
[19] NERC. *Understand and Calculate Frequency Response*. Accessed: Dec. 2018. [Online]. Available: file:///C:/Users/Desong%20Bian/Downloads/Understand%20and%20Calculate%20Frequency%20Response.pdf.pdf
[20] WECC. *System Performance TPL_001_WECC_RBP_2*. Accessed: Dec. 2018. [Online]. Available: https://www.wecc.biz/Reliability/TPL-001-WECC-RBP-2.1.pdf
[21] NERC. *Balancing and Frequency Control*. [Online]. Available: http://www.nerc.com/docs/oc/rs/NERC%20Balancing%20and%20Frequency%20Control%20040520111.pdf
[22] NERC. *M-4 Interconnection Frequency Response*. Accessed: Dec. 2018. [Online]. Available: http://www.nerc.com/pa/RAPA/ri/Pages/InterconnectionFrequencyResponse.aspx
[23] D. Bian, M. Kuzlu, M. Pipattanasomporn and S. Rahman, "Analysis of communication schemes for advanced metering infrastructure (AMI)," in *Proc. IEEE PES Gen. Meeting Conf. Expo.*, National Harbor, MD, USA, Jul. 2014, pp. 1–5
[24] Digikey LLC. *RFI Information*. Accessed: Dec. 2018. [Online]. Available: http://www.digikey.com/Web%20Export/Supplier%20Content/CurtisInd_364/PDF/Curtis_FAQ.pdf?redirected=1
[25] D. Bian, M. Kuzlu, M. Pipattanasomporn, and S. Rahman, "Assessment of communication technologies for a home energy management system," in *Proc. ISGT*, Washington, DC, USA, Feb. 2014, pp. 1–5.
[26] D. S. A. Elminaam, H. M. A. Kader, and M. M. Hadhoud. *Encryption Processing Speed*. Accessed: Dec. 2018. [Online]. Available: http://www.ibimapublishing.com/journals/CIBIMA/volume8/v8n8.pdf

DESONG BIAN (S'12–M'17) received the B.S. degree from the Department of Electrical and Computer Engineering, Tongji University, Shanghai, China, in 2007, the M.S. degree from the Department of Electrical and Computer Engineering, University of Florida, Gainesville, FL, USA, in 2011, and the Ph.D. degree from the School of Electrical and Computer Engineering, Virginia Tech, Arlington, VA, USA, in 2016. He is currently an Engineer with GEIRI North America, San Jose, CA, USA. His research interests include PMU-related applications, demand response, and communication network for smart grid.

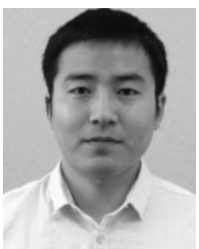

DI SHI (M'12–SM'17) received the B.S. degree in electrical engineering from Xi'an Jiaotong University, Xi'an, China, in 2007, and the M.S. and Ph.D. degrees in electrical engineering from Arizona State University, Tempe, AZ, USA, in 2009 and 2012, respectively. He currently leads the PMU & System Analytics Group, GEIRI North America, San Jose, CA, USA. His research interests include WAMS, energy storage systems, and renewable integration. He is an Editor of the IEEE TRANSACTIONS ON SMART GRID.

MANISA PIPATTANASOMPORN (S'01–M'06–SM'11) received the Ph.D. degree in electrical engineering from Virginia Polytechnic Institute and State University, Blacksburg, VA, USA, in 2004. She joined the Department of Electrical and Computer Engineering, Virginia Polytechnic Institute and State University, as an Assistant Professor, in 2006. She manages multiple research grants from the U.S. National Science Foundation, the U.S. Department of Defense, and the U.S. Department of Energy, on research topics related to smart grid, microgrid, energy efficiency, load control, renewable energy, and electric vehicles. Her research interests include renewable energy systems, energy efficiency, distributed energy resources, and the smart grid.

MURAT KUZLU (M'11–SM'15) joined Old Dominion University, in 2017, as an Assistant Professor. In 2011, he joined Virginia Tech's Advanced Research Institute, Arlington, as a Post-Doctoral Fellow. From 2005 to 2006, he was a Global Network Product Support Engineer with Nortel Networks, Turkey. In 2006, he joined the Energy Institute, TUBITAK-MAM, Turkey, as a Senior Researcher. His research interests include smart grid, demand response, smart metering systems, wireless communication, and embedded systems.

SAIFUR RAHMAN (S'75–M'78–SM'83–F'98) is the Director of the Advanced Research Institute, Virginia Polytechnic Institute and State University, Blacksburg, VA, USA, where he is the Joseph Loring Professor of electrical and computer engineering and also directs the Center for Energy and the Global Environment. He served as the Vice President of the IEEE Publications Board and as a member of the IEEE Board of Governors, in 2006. He is a Distinguished Lecturer of the IEEE Power and Energy Society. He has published in the areas of smart grid, conventional and renewable energy systems, load forecasting, uncertainty evaluation, and infrastructure planning. From 1996 to 1999, he was a Program Director in the engineering directorate of the National Science Foundation. From 2009 to 2013, he served as a Vice President of the IEEE Power and Energy Society and as a member of its Governing Board. He is a Member-at-Large of the IEEE-USA Energy Policy Committee. He is the Editor-in-Chief of the *IEEE Electrification Magazine*.